Electronic Supplementary Information

A robust and water-stable two-fold interpenetrated metal organic framework containing both rigid tetrapodal carboxylate and rigid bifunctional nitrogen linkers exhibiting selective CO_2 capture†

Vijay Gupta and Sanjay K. Mandal*

Department of Chemical Sciences, Indian Institute of Science Education and Research Mohali, Sector 81, Manauli PO, S.A.S. Nagar, Mohali, Punjab 140306, India

Corresponding Author
*E-mail: sanjaymandal@iisermohali.ac.in

Table of Contents

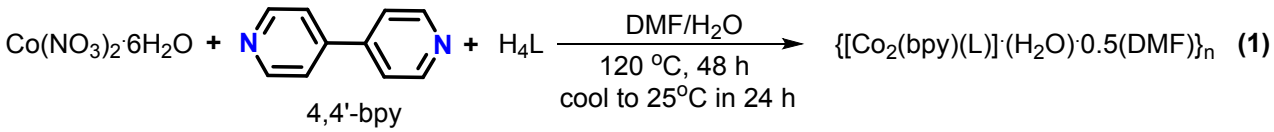

Scheme S1 Solvothermal synthesis of **1**.

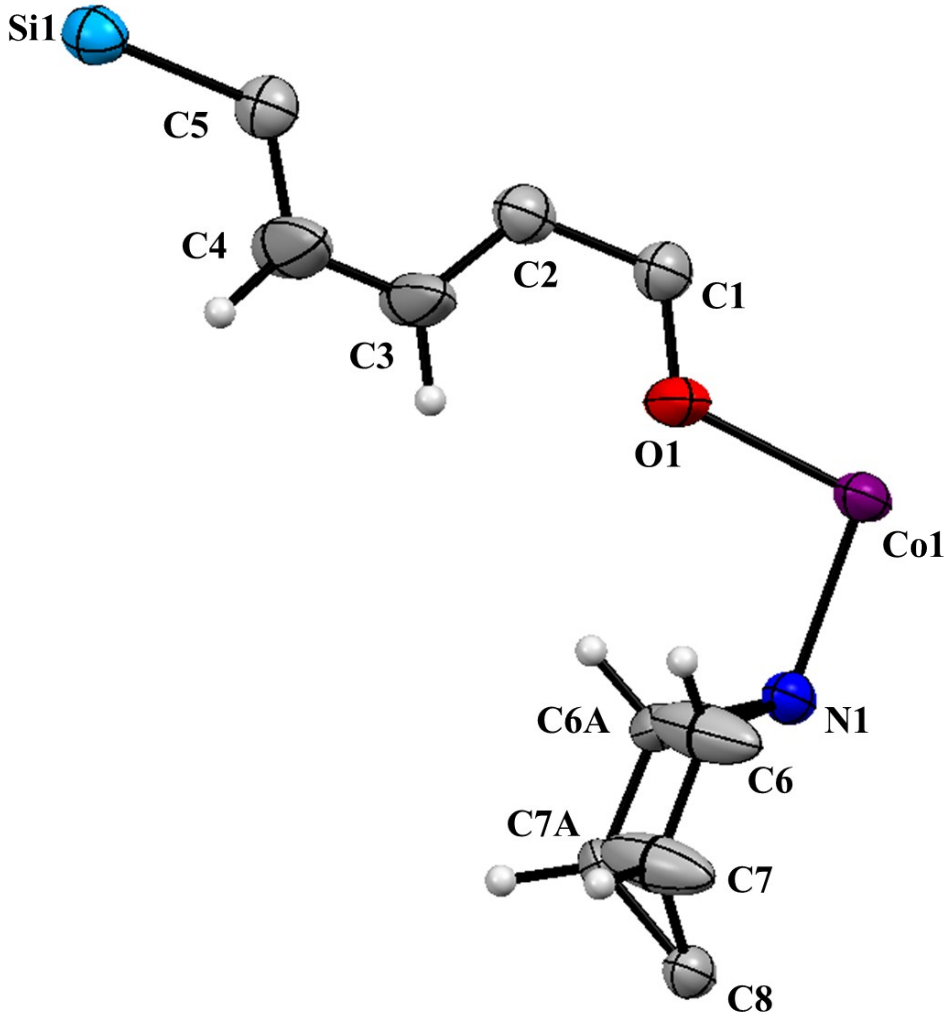

Fig. S1 View of the asymmetric unit in **1**.

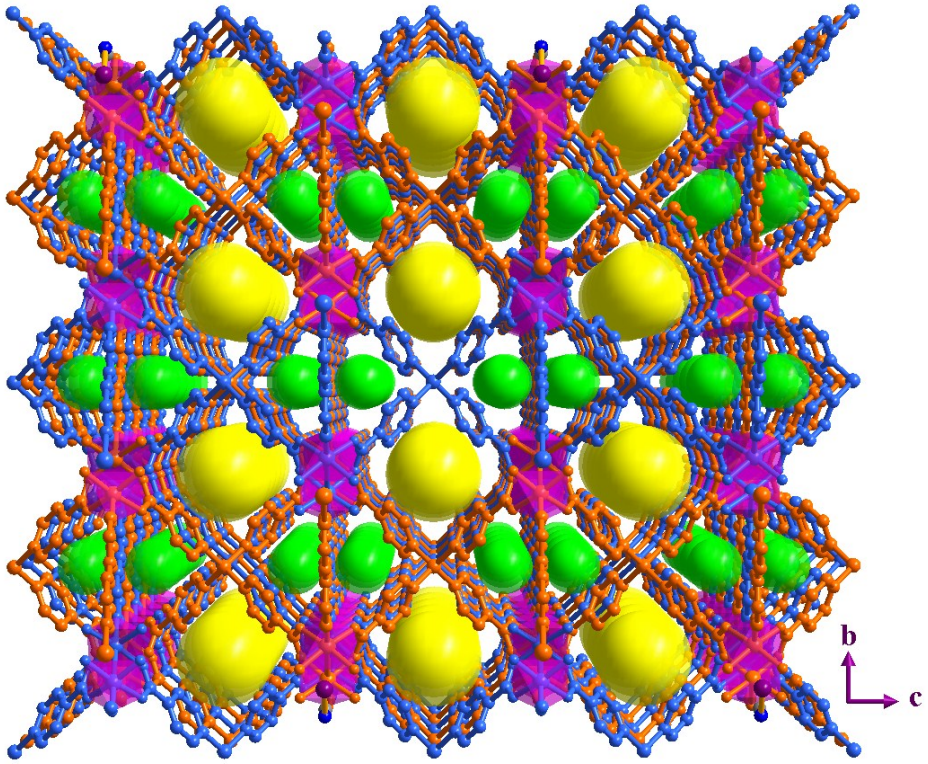

Fig. S2 View of two types of channels in doubly-interpenetrated framework of **1** (along *a*-axis) shown by dummy balls in different colors.

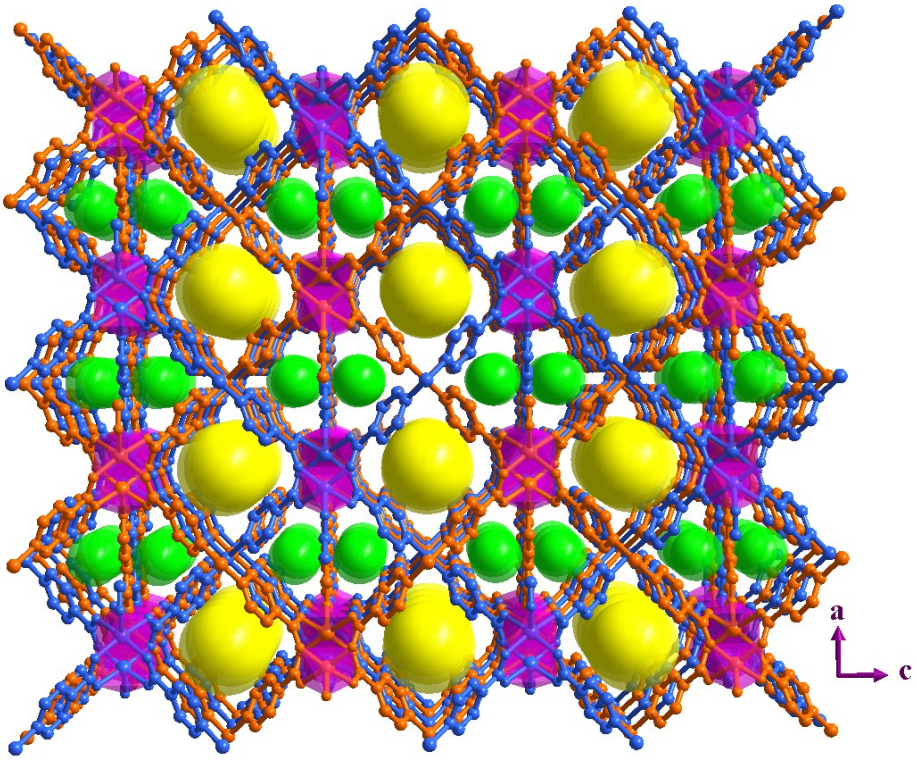

Fig. S3 View of two types of channels in doubly-interpenetrated framework of **1** (along *b*-axis) shown by dummy balls in different colors.

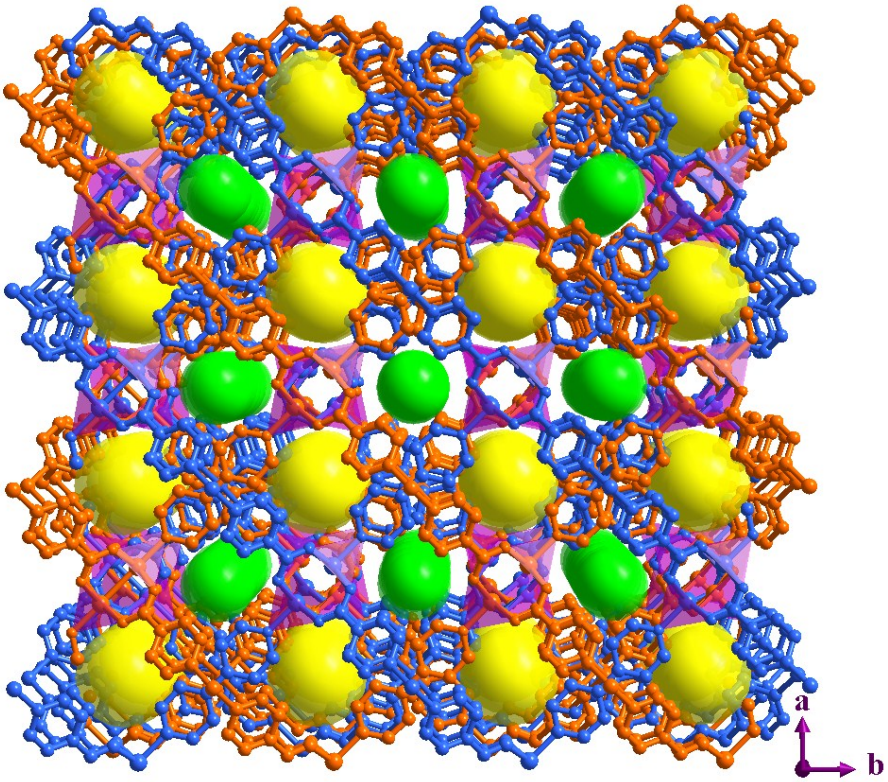

Fig. S4 View of two types of channels in doubly-interpenetrated framework of **1** (along *c*-axis) shown by dummy balls in different colors.

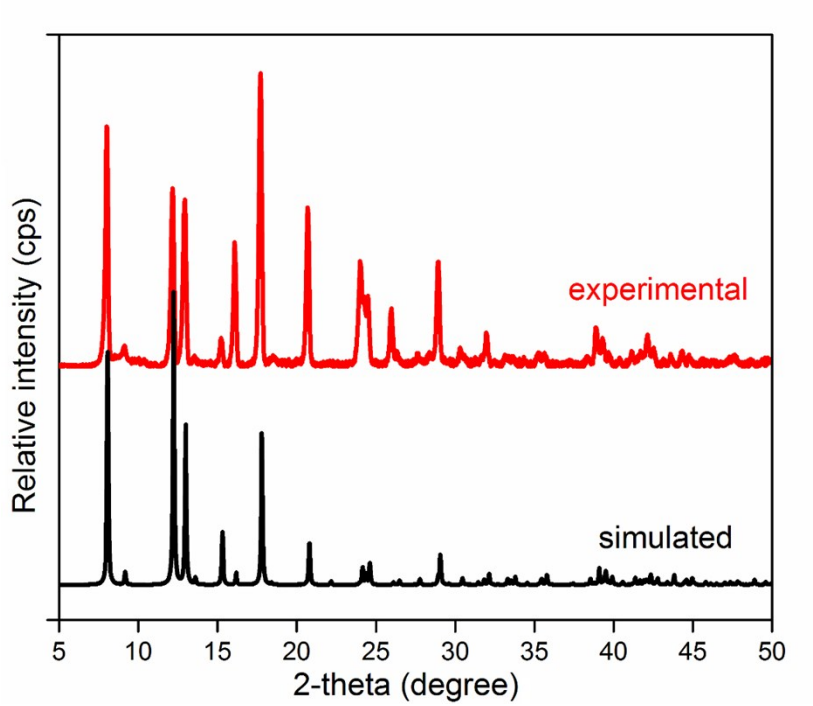

Fig. S5 Simulated (from the single crystal data) and experimental powder X-ray diffraction patterns of **1**.

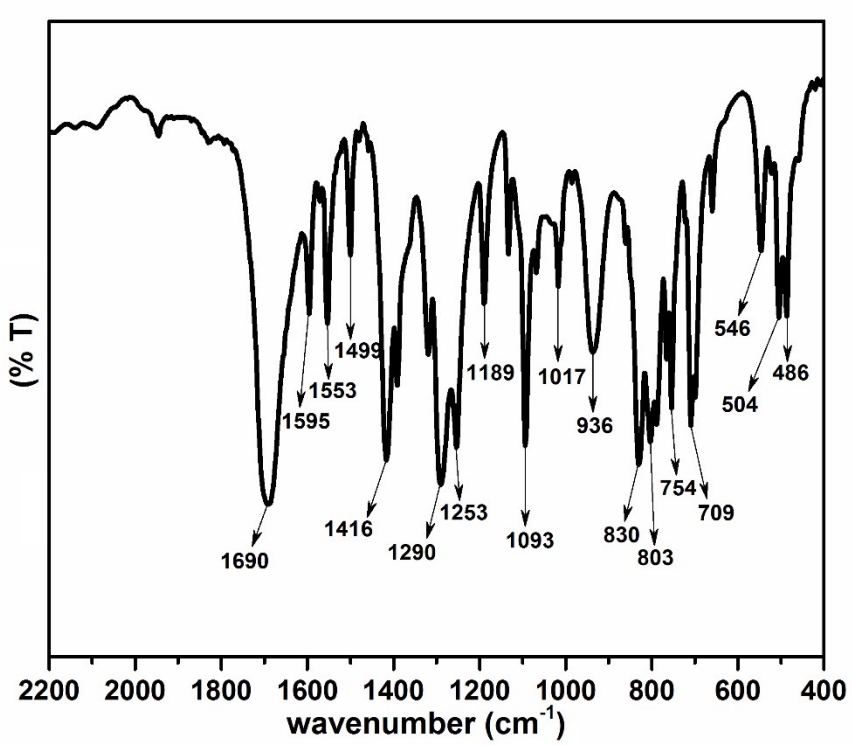

Fig. S6 FTIR spectrum of H_4L.

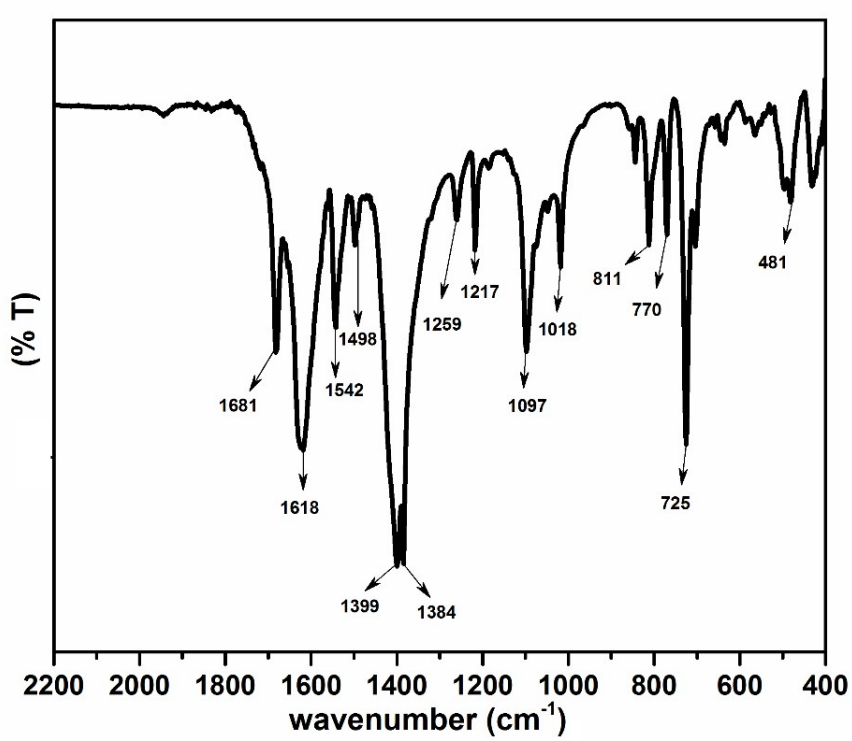

Fig. S7 FTIR spectrum of **1**.

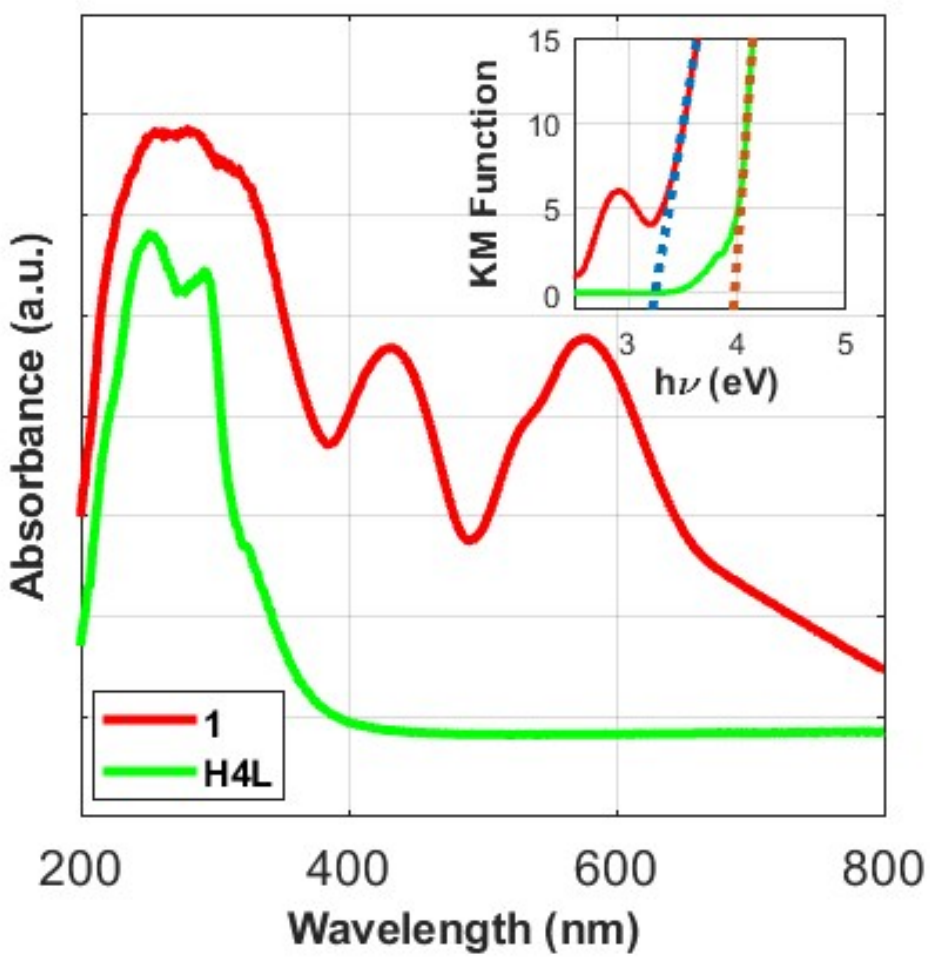

Fig. S8 Diffuse reflectance UV-Vis spectra of **1** (red line) and H_4L (green line); inset: KM function vs. energy (eV) of **1** and H_4L.

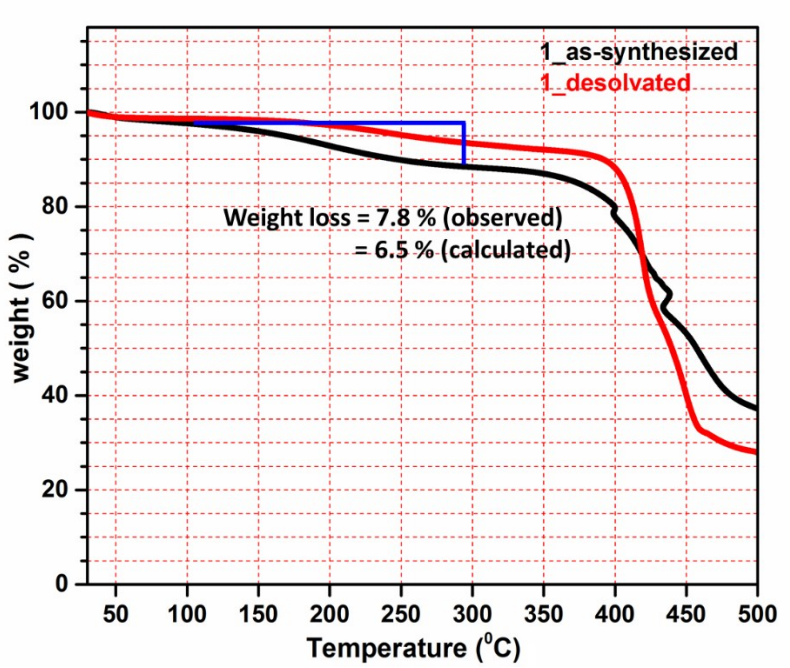

Fig. S9 Thermogravimetric profiles of **1** (as-synthesized and de-solvated).

Calculation of determining solvent molecules squeezed out:

Number of electrons squeezed out = 31

Number of electrons in (1 H_2O + 0.5 DMF) molecule = (10 +20) = 30; this is in good agreement with the number of electrons squeezed out (31).

Support from the TGA analysis:

% weight loss due to (1 H_2O + 0.5 DMF) molecule = (54.5/836) × 100 = 6.51 %; this is in good agreement with the experimental value (7.8 %).

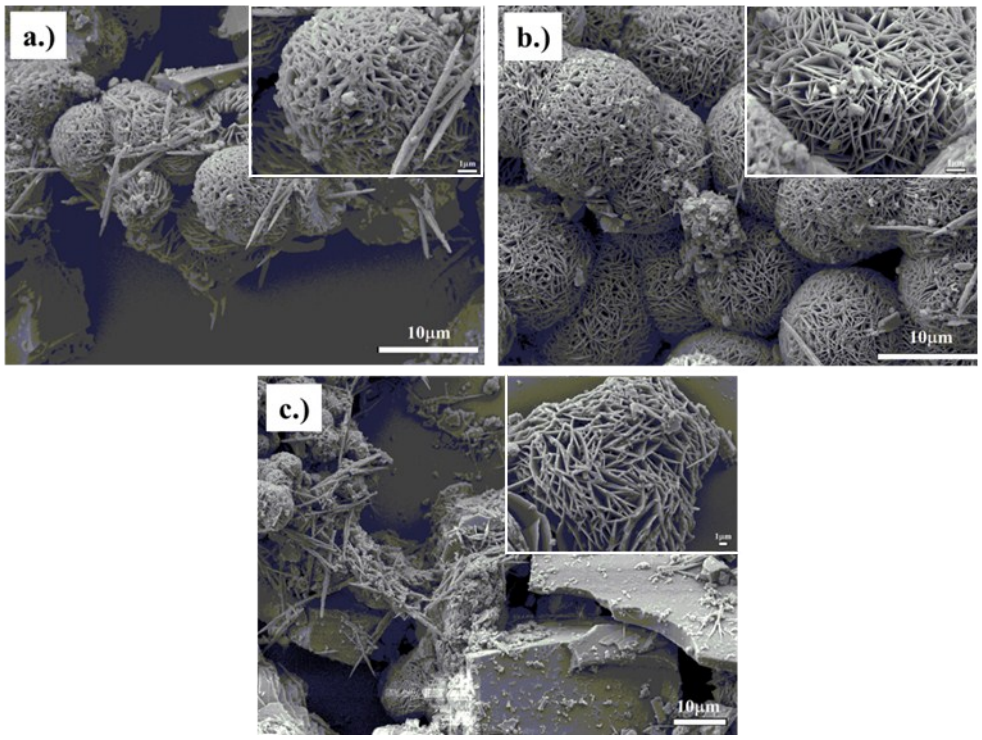

Fig. S10 FESEM images for the (a) as-synthesized sample of **1**, (b) after water stability test and (c) after heating the as-synthesized sample of **1** up to 300 °C.

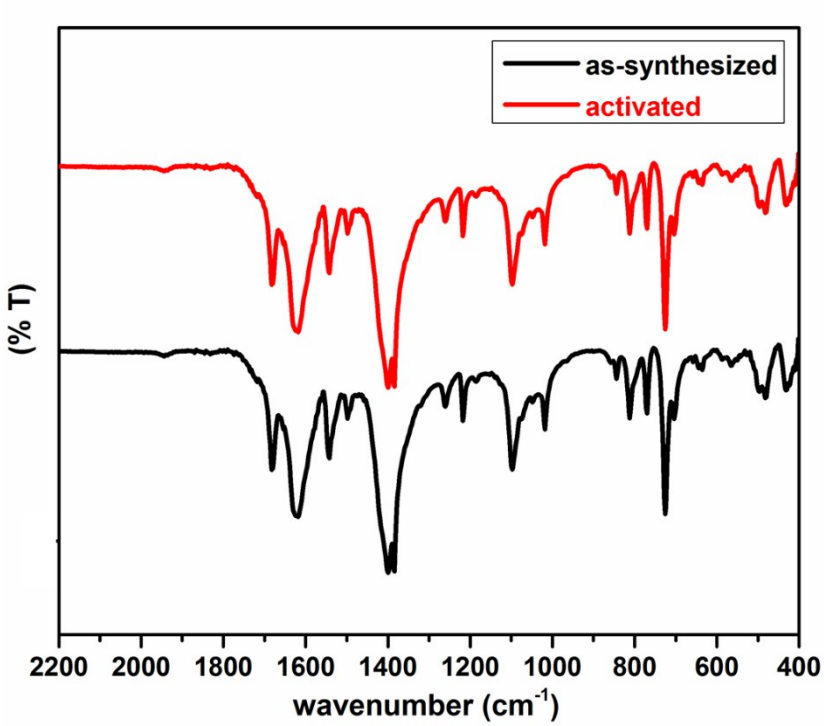

Fig. S11 FTIR spectra of activated and as-synthesized sample of **1**.

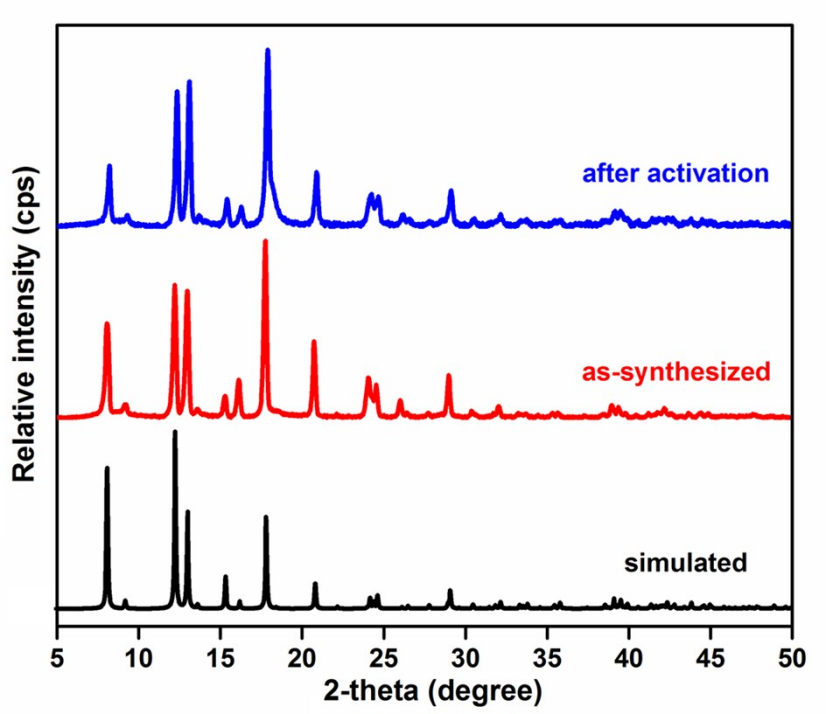

Fig. S12 Comparison of the PXRD patterns: after activation of **1**, as-synthesized **1** and simulated from single crystal data, indicating retention of crystallinity and phase purity after the activation process.

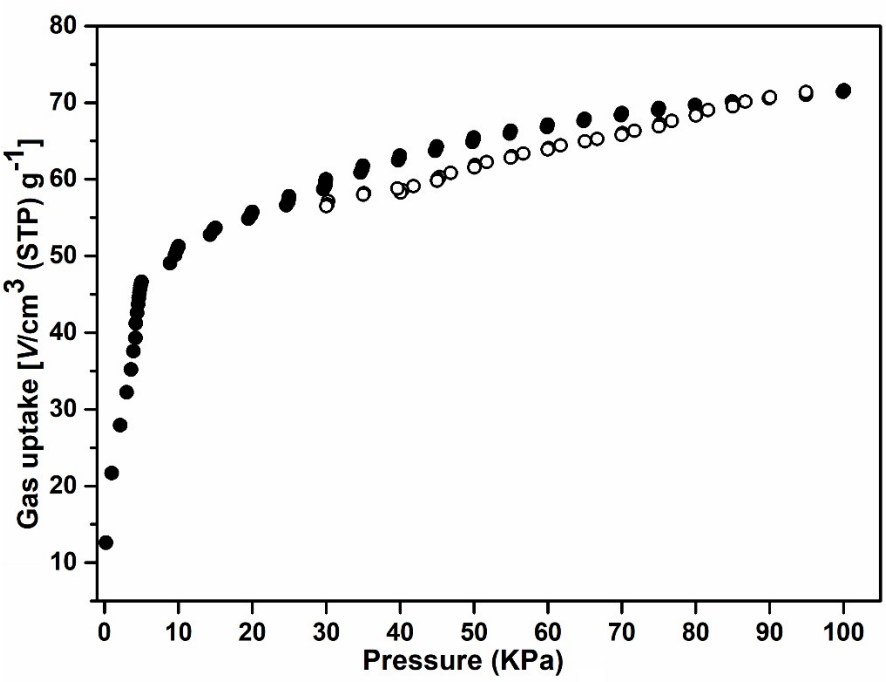

Fig. S13 CO_2 sorption isotherm for **1** at 195 K. Filled circles and open circles indicate the adsorption and desorption points, respectively.

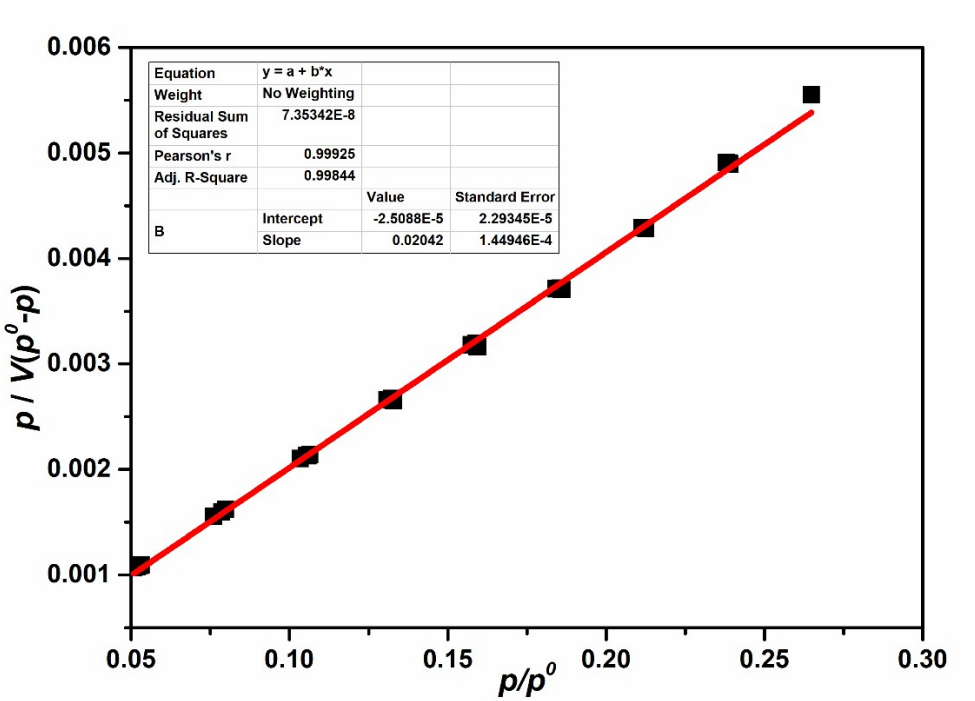

S_{BET} = {[1 / (0.02042 + (-0.000025088))] / 22414} x 6.023 x 10^{23} x 0.170 x 10^{-18} = 224 m^2g^{-1}.

Fig. S14 BET surface area of **1** obtained from the CO_2 adsorption isotherm at 195 K.

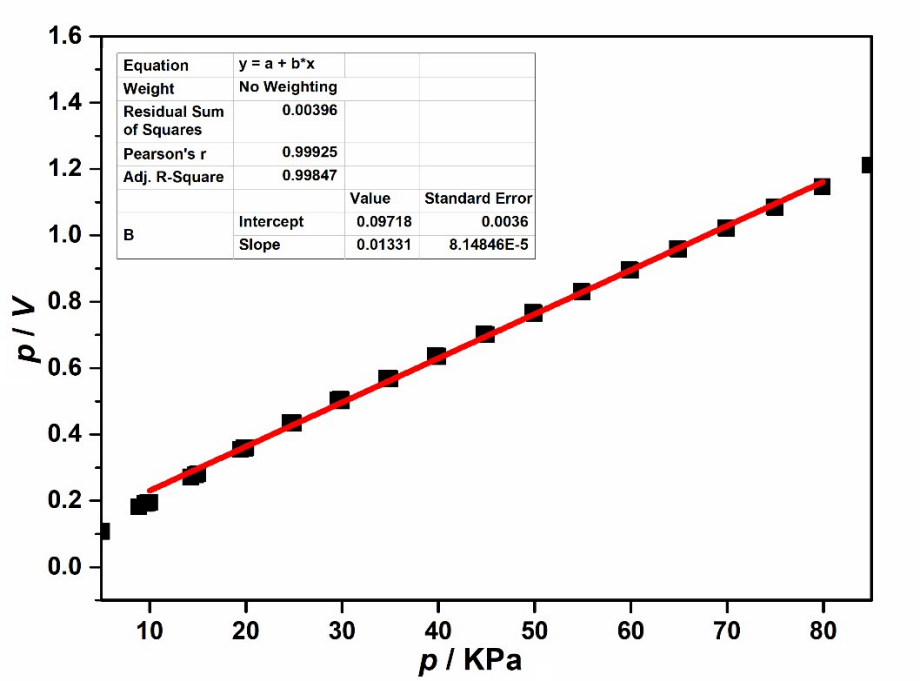

$S_{Langmuir}$ = [(1 / 0.01331) / 22414] x 6.023 x 10^{23} x 0.170 x 10^{-18} = 343 m^2g^{-1}.

Fig. S15 Langmuir surface area of **1** obtained from the CO_2 adsorption isotherm at 195 K.

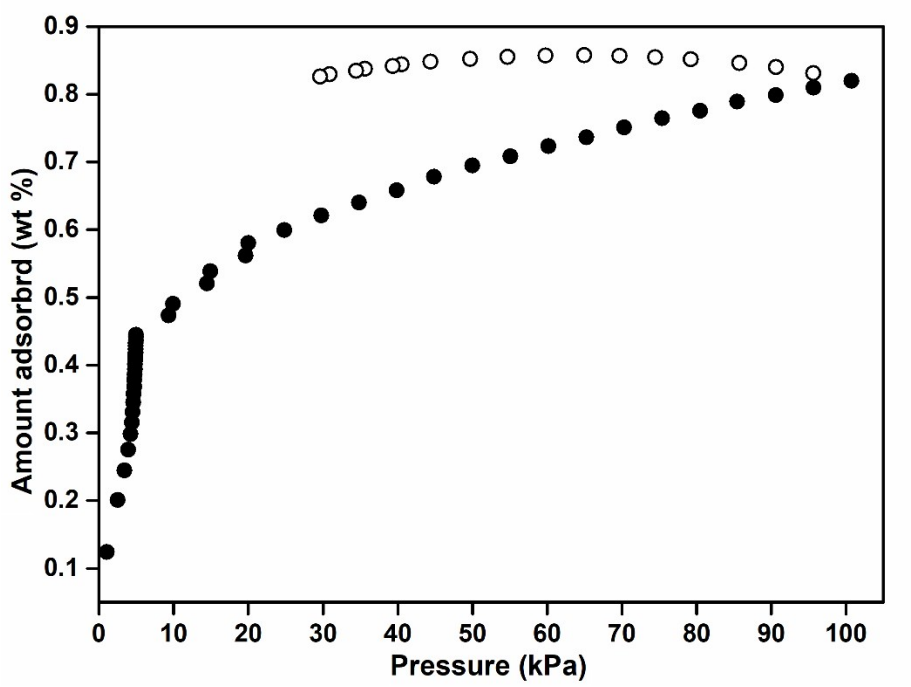

Fig. S16 H_2 sorption isotherm for **1** at 77 K. Filled circles and open circles indicate the adsorption and desorption points, respectively.

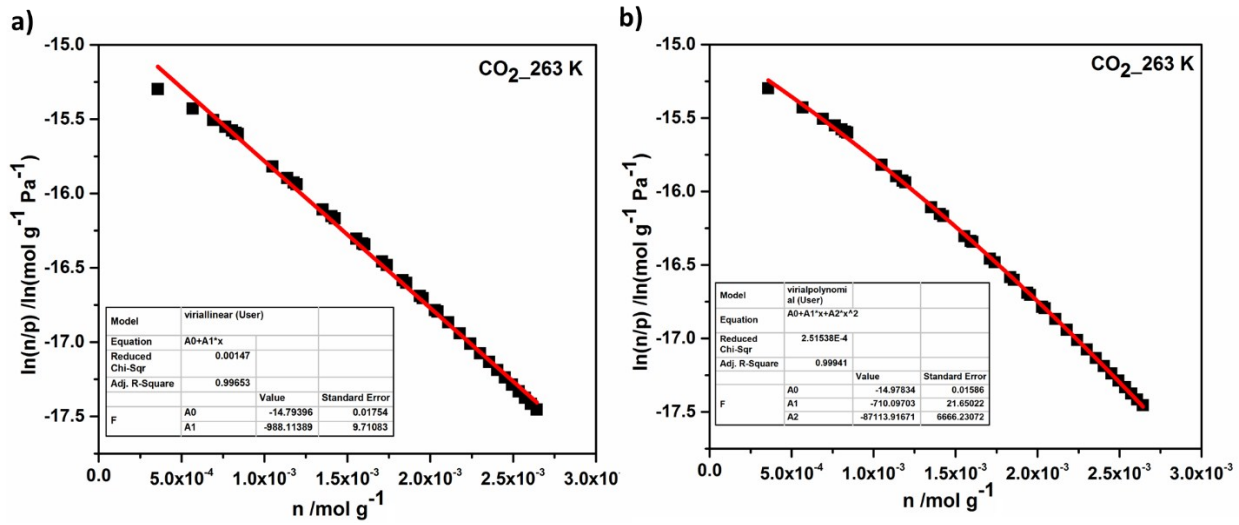

Fig. S17 Virial graphs analysis (linear: $\ln(n/P) = A_0 + A_1n$ and polynomial: $\ln(n/P) = A_0 + A_1n + A_2n^2$) for CO_2 adsorption isotherms of **1** at 263 K: (a) linear equation and (b) polynomial equation.

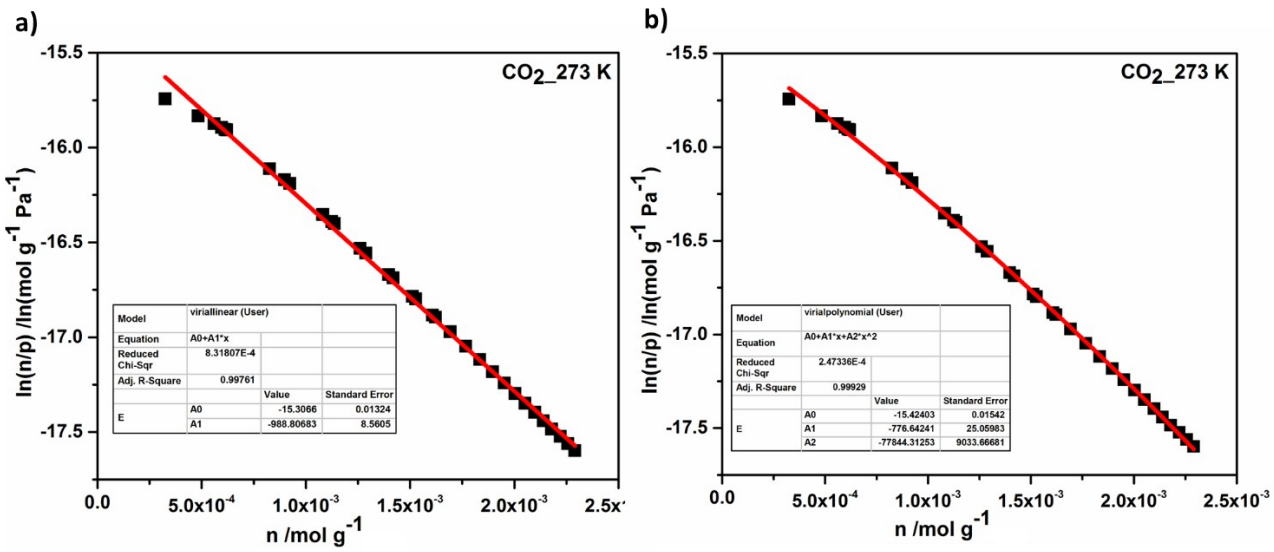

Fig. S18 Virial graphs analysis (linear: $\ln(n/P) = A_0 + A_1n$ and polynomial: $\ln(n/P) = A_0 + A_1n + A_2n^2$) for CO_2 adsorption isotherms of **1** at 273 K: (a) linear equation and (b) polynomial equation.

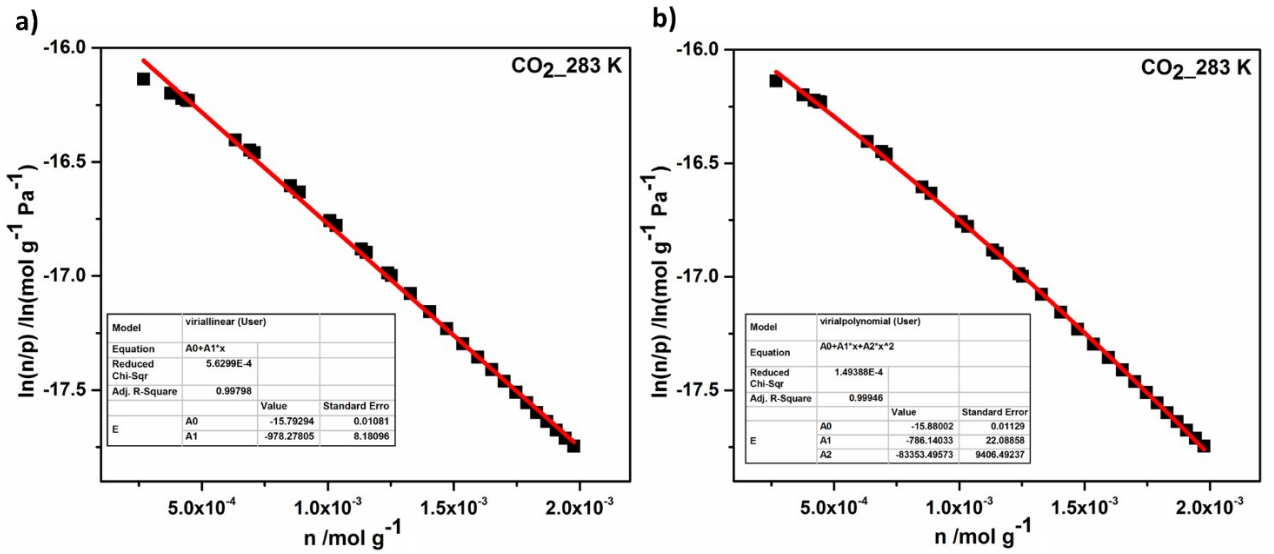

Fig. S19 Virial graphs analysis (linear: $\ln(n/P) = A_0 + A_1n$ and polynomial: $\ln(n/P) = A_0 + A_1n + A_2n^2$) for CO_2 adsorption isotherms of **1** at 283 K: (a) linear equation and (b) polynomial equation.

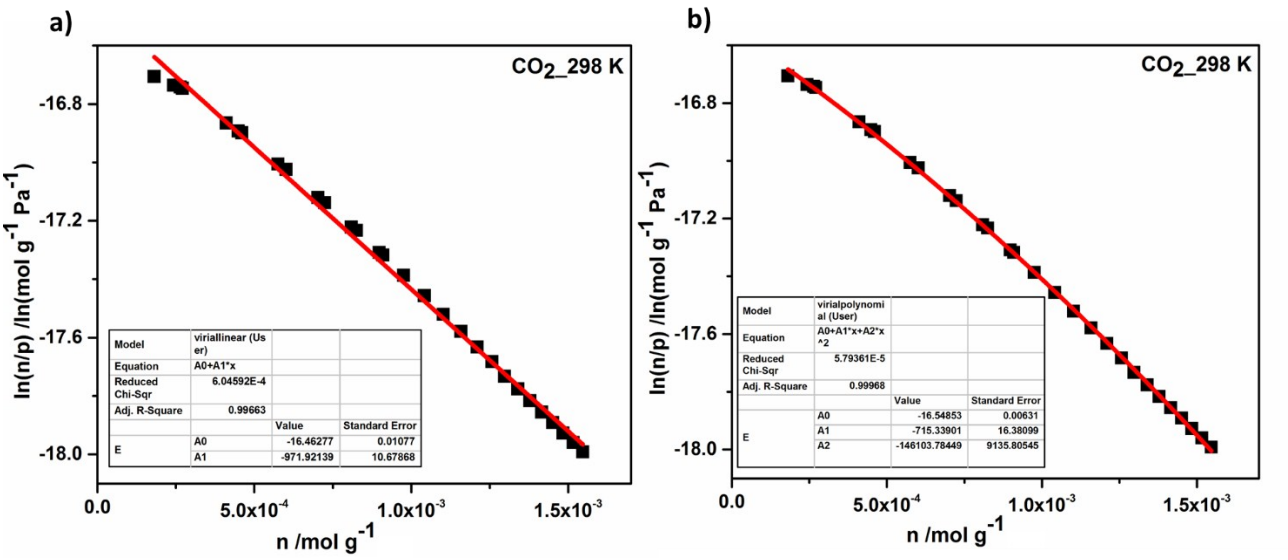

Fig. S20 Virial graphs analysis (linear: $\ln(n/P) = A_0 + A_1n$ and polynomial: $\ln(n/P) = A_0 + A_1n + A_2n^2$) for CO_2 adsorption isotherms of **1** at 298 K: (a) linear equation and (b) polynomial equation.

Table S1 Fitting parameters for virial graph analysis of **1**.

Isotherm	Linear fit			Polynomial fit			
	A_0	A_1	R^2	A_0	A_1	A_2	R^2
CO_2 (263 K)	-14.79396 ±0.01754	-988.11389 ±9.71083	0.99653	-14.97834 ±0.01586	-710.09703 ±21.65022	-87113.91671 ±6666.23072	0.99941
CO_2 (273 K)	-15.3066 ±0.01324	-988.80683 ±8.5605	0.99761	-15.42403 ±0.01542	-776.64241 ±25.05983	-77844.31253 ±9033.66681	0.99929
CO_2 (283 K)	-15.79294 ±0.01081	-978.27805 ±8.18096	0.99798	-15.88002 ±0.01129	-786.14033 ±22.08858	-83353.49573 ±9406.49237	0.99946
CO_2 (298 K)	-16.46277 ±0.01077	-971.32139 ±10.67868	0.99663	-16.54853 ±0.00631	-715.33901 ±16.38099	-146103.7844 ±9135.80545	0.99968

The isosteric adsorption heat at zero coverage ($Q_{st,0}$) was calculated from the gradient of plotting A_0 against 1/T, i.e., $\partial A0/\partial (1/T) = Q_{st,0}/R$ (R = 8.314 J K^{-1} mol^{-1}).

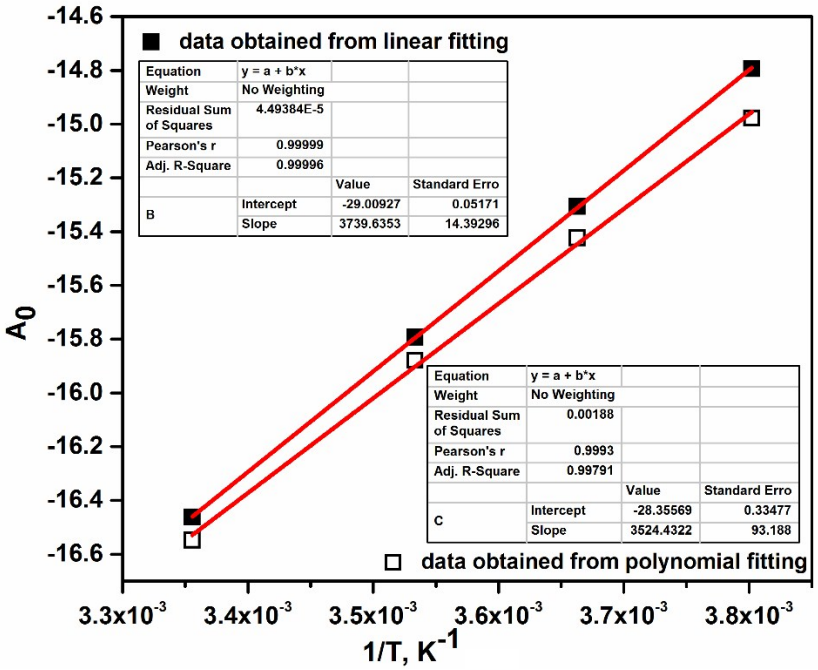

Fig. S21 Variation of virial parameter A_0 with 1/T for **1**. The isosteric heat ($Q_{st,0}$) of adsorption at zero surface coverage was calculated from the gradient of the straight line. The polynomial fitting of ln (n/p) vs n gives value of 29.30 ± 0.77 kJ mol^{-1}; as a comparison, linear fitting gives 31.09 ± 0.11 kJ mol^{-1}.

Calculation of CO_2/N_2 and CO_2/CH_4 Selectivity:

Adsorption isotherms and gas selectivities of mixed CO_2/N_2 (15:85) and CO_2/CH_4 (50:50) at different temperatures were calculated based on the ideal adsorbed solution theory (IAST) proposed by Myers and Prausnitz. The IAST theory assumes that the adsorbed phase is a two-dimensional solution in equilibrium with the gas phase. Both the components in the mixture behave as ideal adsorbed solution and conform to the rule analogous to Raoult's law. In order to calculate the selective sorption performance of **1** toward the separation of binary mixed gases, the parameters fitted from the single-component CO_2, CH_4 and N_2 adsorption isotherms based on the single-site Langmuir-Freundlich equation as given below.

$$Q = Q_{sat}\left(\frac{Kc^n}{1 + Kc^n}\right)$$

where Q is the adsorbed amount (mmol/g), Q_{sat} is the saturation capacity (mmol/g), c is the equilibrium pressure (kPa), and K and 1/n are the Langmuir and Freundlich constants.

Then the fitted parameters were used to predict the molar fraction of A in the adsorbed phase using following equation:

$$Q_{sat,a} ln\left(1 + \frac{K_a c^{n_a} y}{x}\right) - Q_{sat,b} ln\left(1 + \frac{K_b c^{n_b} (1-y)}{(1-x)}\right) = 0$$

where $Q_{sat,a}$, K_a and n_a are the Langmuir-Freundlich fitting parameters of adsorption equilibrium of pure A, $Q_{sat,b}$, K_b and n_b are Langmuir-Freundlich parameters of adsorption equilibrium of pure B, and x and y are the molar fractions of A in the adsorbed phase and in bulk phase, respectively. The predicted adsorption selectivity is defined as

$$S = \left(\frac{x_1/y_1}{x_2/y_2}\right)$$

where x_i is the mole fractions of component i in the adsorbed and y_i is the mole fractions of component i in bulk phase. The IAST calculations were carried out for a binary mixture containing 15% CO_2 (y_1) and 85% N_2 (y_2), which is typical of flue gases and for a binary mixture containing 50% CO_2 (y_1) and 50% CH_4 (y_2), which is typical of landfill gases.

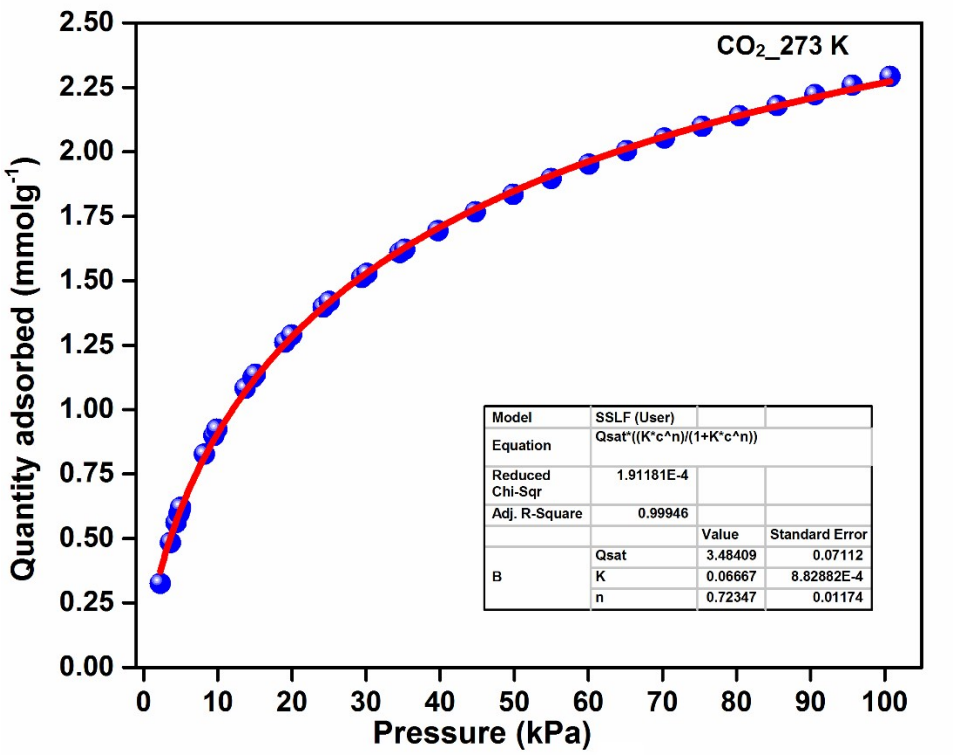

Fig. S22 Fitting of CO_2 adsorption points collected at 273 K by Langmuir Freundlich adsorption model.

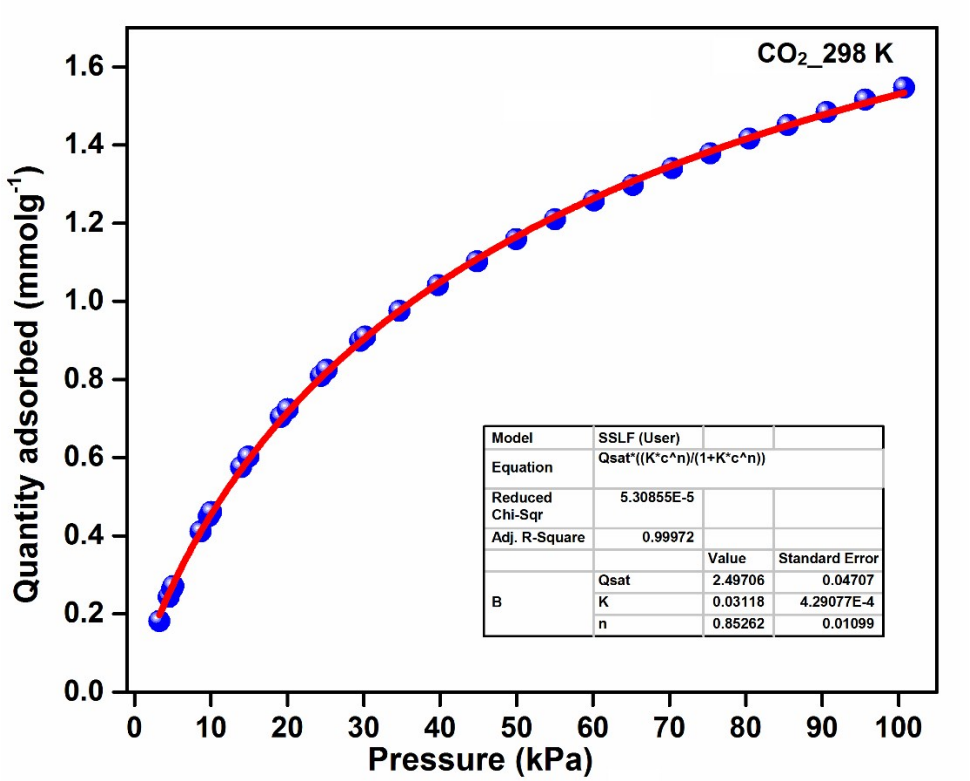

Fig. S23 Fitting of CO_2 adsorption points collected at 298 K by Langmuir-Freundlich adsorption model.

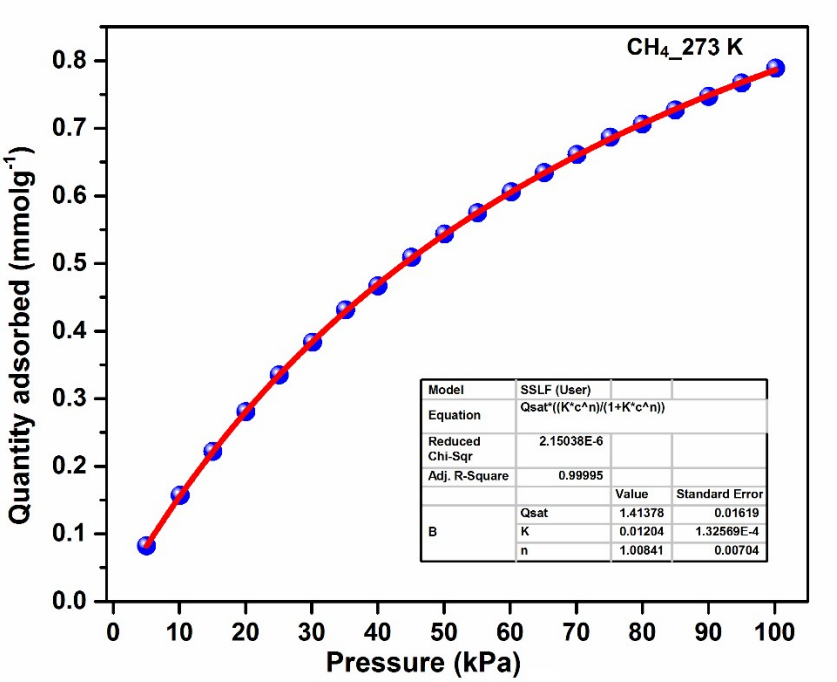

Fig. S24 Fitting of CH_4 adsorption points collected at 273 K by Langmuir Freundlich adsorption model.

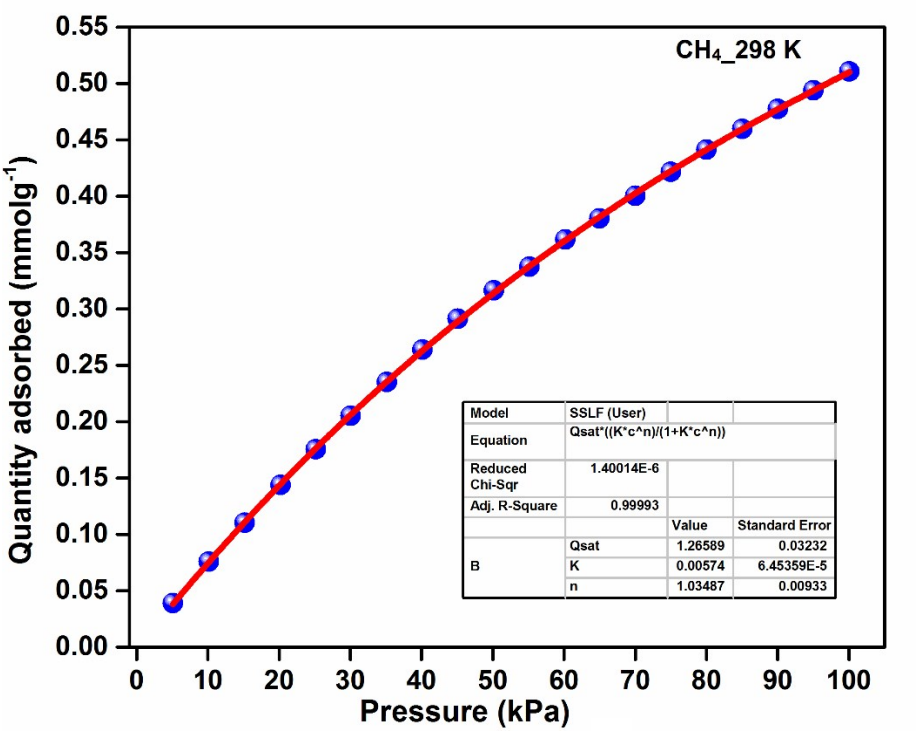

Fig. S25 Fitting of CH_4 adsorption points collected at 298 K by Langmuir-Freundlich adsorption model.

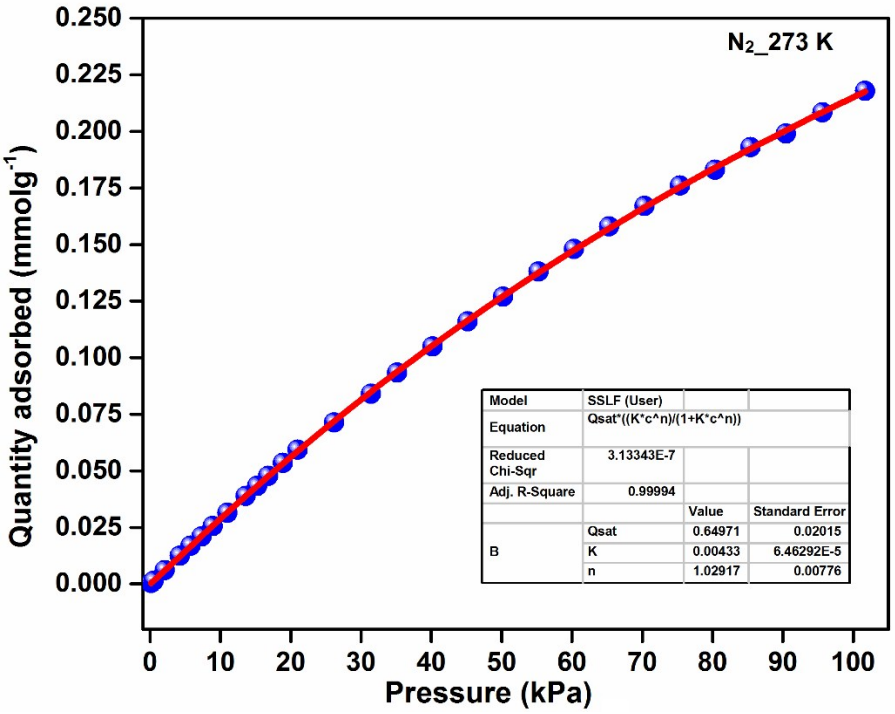

Fig. S26 Fitting of N_2 adsorption points collected at 273 K by Langmuir-Freundlich adsorption model.

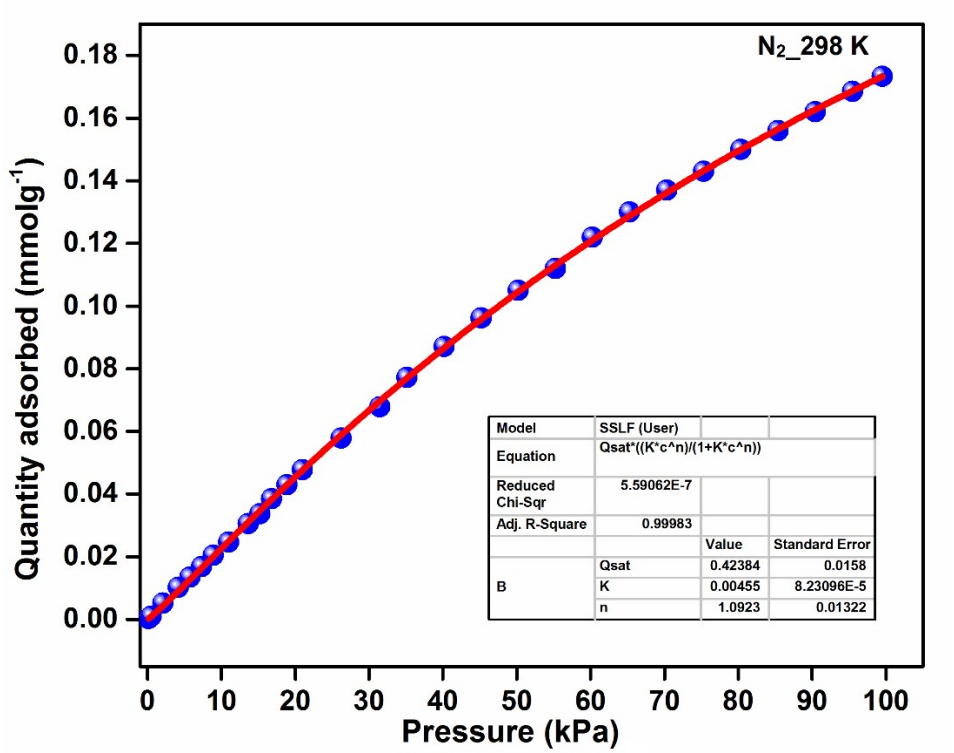

Fig. S27 Fitting of N_2 adsorption points collected at 298 K by Langmuir-Freundlich adsorption model.

Table S2 Fitting parameters for Langmuir-Freundlich fits.

Isotherm	Langmuir Frundlich equation: q = Qsat*[K*c^n/(1+K*c^n)]			
	Qsat	K	n	R^2
CO_2 (273 K)	3.48409 ±0.07112	0.06667 ±8.82882E-4	0.72347 ±0.001174	0.99946
CH_4 (273 K)	1.41378 ±0.01619	0.01204 ±1.32569E-4	1.00841 ±0.00704	0.99993
N_2 (273 K)	0.64971 ±0.02015	0.00433 ±6.46292E-5	1.02917 ±0.00776	0.99994
CO_2 (298 K)	2.49706 ±0.04707	0.03118 ±4.29077E-4	0.85262 ±0.01099	0.99972
CH_4 (298 K)	1.26589 ±0.03232	0.00574 ±6.45359E-5	1.03487 ±0.00933	0.99993
N_2 (298 K)	0.42384 ±0.0158	0.00455 ±8.23096E-5	1.0923 ±0.01322	0.99994

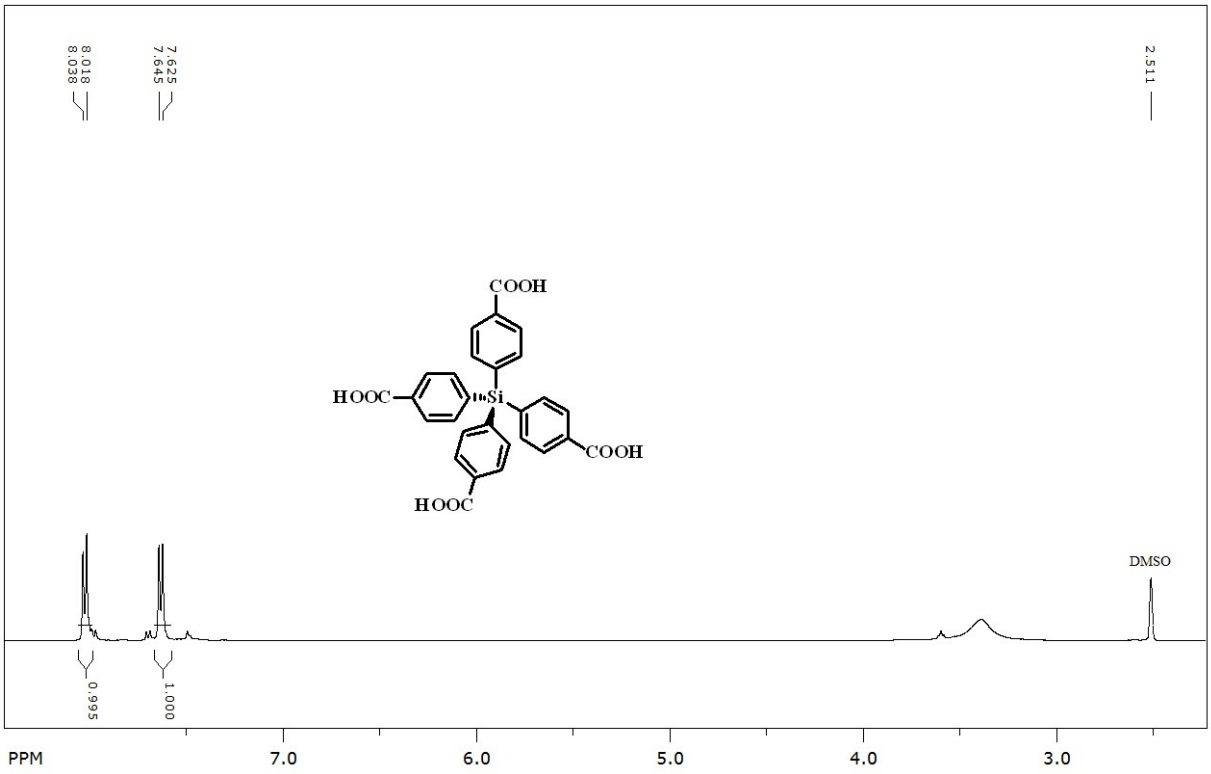

Fig. S28 ^{1}H NMR spectrum of H_4L in DMSO-d_6.

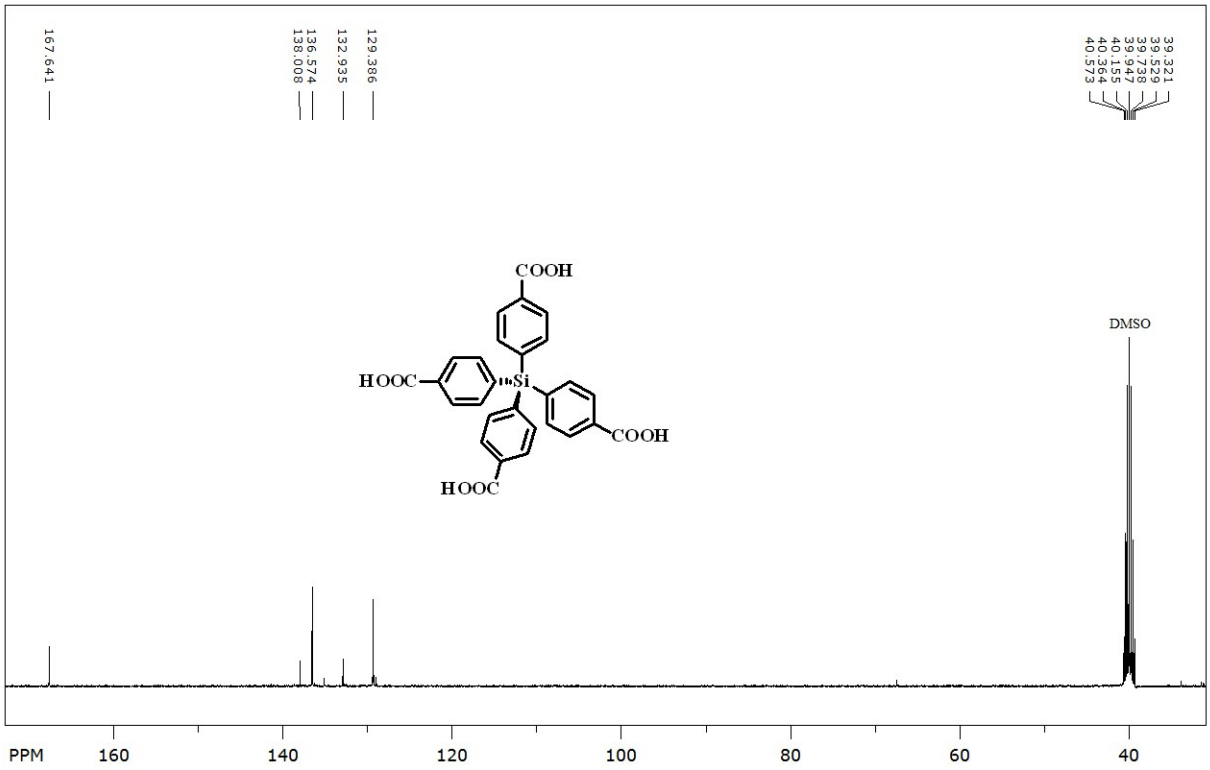

Fig. S29 ^{13}C NMR spectrum of H_4L in DMSO-d_6.

Table S3 Single crystal data and refinement parameters for **1**.

Chemical Formula	$C_{38}H_{24}Co_2N_2O_8Si$
Formula Weight	782.54 g/mol
Temperature (K)	100(2)
Wavelength (Å)	0.71073
Crystal System	tetragonal
Space Group	$P4_2/mcm$
a (Å)	9.6299(5)
b (Å)	9.6299(5)
c (Å)	21.8959(12)
α (°)	90
β (°)	90
γ (°)	90
Z	2
V (Å^3)	2030.52(2)
Density (mg/cm3)	1.280 g/cm^3
μ(mm^{-1})	0.894
F(000)	796
Theta (°) Range for Data Coll.	2.82 to 25.08
Reflections Collected	34835
Independent Reflections	1025
Reflections with I >2σ(I))	896
R_{int}	0.0957
No. of Parameters refined	91
GOF on F^2	1.151
Final R_1[a]/wR_2[b] (I >2σ(I))	0.0674/0.1605
Weighted R_1/wR_2(all data)	0.0769/0.1655
Largest diff. peak	0.45
and hole(eÅ^{-3})	-0.41

[a]$R1 = \Sigma||F_o| - |F_c||/\Sigma|F_o|$. [b]$wR_2 = [\Sigma w(F_o^2 - F_c^2)^2/\Sigma w(F_o^2)^2]^{1/2}$, where $w = 1/[\sigma^2(F_o^2) + (aP)^2 + bP]$, $P = (F_o^2 + 2F_c^2)/3$

Table S4 Selected bond lengths (Å) and angles (deg) for **1**.

Bond lengths			
Co(1)-O(1)	2.009(3)	Co(1)-O(1)#2	2.009(3)
Co(1)-O(1)#3	2.009(3)	Co(1)-O(1)#4	2.009(3)
Co(1)-N(1)	2.026(7)		
Bond Angles			
O(1)···Co(1)···O(1)#2	91.1(2)	O(1)···Co(1)···O(1)#3	169.02(17)
O(1)···Co(1)···O(1)#4	87.9(2)	O(1)#2···Co(1)···O(1)#3	87.9(2)
O(1)#2···Co(1)···O(1)#4	169.01(17)	O(1)#3···Co(1)···O(1)#4	91.1(2)
O(1)···Co(1)···N(1)	95.49(9)	O(1)#2···Co(1)···N(1)	95.49(9)
O(1)#3···Co(1)···N(1)	95.49(9)	O(1)#4···Co(1)···N(1)	95.49(9)
O(1)···Co(1)···Co(1)#1	84.51(9)	O(1)#2···Co(1)···Co(1)#1	84.51(9)
O(1)#3···Co(1)···Co(1)#1	84.51(9)	O(1)#4···Co(1)···Co(1)#1	84.51(9)
N(1)···Co(1)···Co(1)#1	180.0		

Symmetry codes:
(#1) 'x, y, z', (#2) '-y, x, z+1/2', (#3) 'y, -x, z+1/2', (#4) 'x, -y, -z+1/2'
(#5) '-x, y, -z+1/2', (#6) '-x, -y, z', (#7) 'y, x, -z', (#8) '-y, -x, -z'
(#9) '-x, -y, -z', (#10) 'y, -x, -z-1/2', (#11) '-y, x, -z-1/2', (#12)'-x, y, z-1/2'
(#13) 'x, -y, z-1/2', (#14) 'x, y, -z', (#15) '-y, -x, z', (#16) 'y, x, z'

Table S5 Q_{st} values of reported MOFs.

Compound	Q_{st} ($kJmol^{-1}$)	Reference
1	**31.09**	**This work**
UTSA-72a	34.6	S1
IITKGP-8	35	S2
IITKGP-6	23	S3
IITKGP-5	22.6	S4
M'MOF-20a	28.4	S5
ROD 6	20-21	S6
ROD 7	26-22	S6
NU 1000	17	S7
PMF-NOTT-1	33.09	S8
PMF- NOTT-2	31.86	S8
$[Zn_2(L)(2,6\text{-}NDC)_2]$	23.3	S9
$[Cd_2(L)(2,6\text{-}NDC)_2]$	28.1	S9
ZnPC-2	32	S10
Cu-BCPPM	29	S11
SIFSIX-3-Zn	45	S12
$[Co_2(tzpa)(OH)(H_2O)_2]$	38.5	S13
$[Cu_2(L)(H_2O)_2]$	36.4	S14
SNU-77H	19.9	S15
NJU-Bai13	21.2	S16
CuBTTri	21	S17[17]
Cu-TDPAT	42.2	S18
[Cu(Me-4py-trz-ia)]	30	S19
[Zn(BTZ)]	31.2	S20
Mg-DOBDC	47	S21

Table S5 Q_{st} values of reported MOFs (cont.)

Ni-DOBDC	41	S21
Co-DOBDC	37	S21
MOF-5	16.5	S22
UMCM-1	11.9	S23
ZJNU-54a	24.7	S24
PCN 88	27	S25
JUC-199	29	S26
MIL-53 (Al)	20.1	S27
HKUST-1	30	S28
NOTT 140a	24.7	S29
MIL-100	63	S30
CuBTTri-en	90	S17
NOTT 202a	22	S31

Table S6 Adsorption selectivity of reported MOFs for CO_2/N_2 (15:85) and CO_2/CH_4 (50:50) at 1 bar.

Compound	CO_2/N_2 adsorption selectivity	CO_2/CH_4 adsorption selectivity	Temperature (K)	Reference
1	**70.5**	**9.9**	**298**	**This work**
	194.7	**19.0**	**273**	**This work**
HKUST-1	101[b]	7.4[a,d]	293	S28
HKUST-1(hydrated)	28[a]	7.5[a]	298	S32
PCN-88a	18[a]	5[a]	296	S25
PCN-61a	15[a]	NA	298	S33
UTSA-15a	NA	14.2[a,d]	296	S34
UTSA-16a	314.7[a]	29.8[a,d]	296	S34
UTSA-20a	NA	8.3[a,d]	296	S34
UTSA-25a	NA	9.4[a,d]	296	S34
UTSA-33a	NA	7.0[a,d]	296	S34
UTSA-34a	NA	5.1[a,d]	296	S34
UTSA-49a	95.8[a]	33.7[a]	298	S35
	197.7[a]	34.8[a]	273	
UTSA-72a	48.3[a]	40.7[a]	273	S36
	35.6[a]	9.3[a]	296	
UTSA-85a	55[a]	11.4[a]	273	S37
	62.5[a]	6.4[a]	296	
ZIF-68	18.7[c]	5[c]	298	S38
ZIF-69	19.9[c]	5.1[c]	298	S38
ZIF-70	17.3[c]	5.2[c]	298	S38
ZIF-78	41.4[a]	10.4[a,d]	296	S38
	50.1[c]	10.6[c]	298	S38
ZIF-79	23.2[c]	5.4[c]	298	S38
ZIF-81	23.8[c]	5.7[c]	298	S38
ZIF-82	35.3[c]	9.6[c]	298	S38
ZIF-95	18±1.7[c]	4.3±0.4[c]	298	S38
ZIF-100	25±2.4[c]	5.9±0.4[c]	298	S38
IITKGP-8	106[a]	17.7[a]	273	S2
	43.7[a]	17.1[a]	295	
IITKGP-7	57[a]	8.4[a]	273	S39
	121.4[a]	8.8[a]	295	
IITKGP-6	51.3[a]	36[a]	273	S3
	42.8[a]	5.1[a]	295	
IITKGP-5	435.5[a]	151.6[a]	273	S4
	147.8[a]	23.8[a]	295	
SIFSIX-1-Cu	27[a]	11[a]	298	S12
SIFSIX-2-Cu	13.7[a]	5.3[a]	298	S12
SIFSIX-2-Cu-i	140[a]	33[a]	298	S12

Table S6 Adsorption selectivity of reported MOFs for CO_2/N_2 (15:85) and CO_2/CH_4 (50:50) at 1 bar (cont.)

TIFSIX-1-Cu	30[a]	11[a]	298	S40
SNFSIX-1-Cu	22[a]	12[a]	298	S40
Cu-BTTri	21[a]	NA	298	S17
en-Cu-BTTri	25[a]	NA	298	S17
mmen-Cu-BTTri	327[a]	NA	298	S41
mmen-Mg_2(dobpdc)	329[a]	NA	298	S42
$Cu_{24}(TPBTM)_8$	22[a]	NA	298	S33
Zn_2(HDDCBA)	NA	8.9[a]	273	S43
	NA	8.1[a]	298	
Cu-TDPAT	57.8[a]	13.8[a,d]	296	S34
Mg-MOF-74	182.1[a]	105.1[a,d]	296	S34
Zn-MOF-74	87.7[a]	5[a]	296	S34
MOF-177	3.6[a]	NA	296	S34
Bio-MOF-11	79.5[a]	NA	296	S34
In_2X	250[a]	6.4[a]	273	S44
	NA	5.6[a]	298	
[ZnLi(PTCA)]	126[a]	26[a]	298	S45
	277[a]	35[a]	273	
MIL-101	NA	9.6[a,d]	296	S34
	NA	5.6[a]	298	
ZJNU-44a	15[a]	5.5[a]	296	S46
PMOF-3a	29.2[a]	8[a]	273	S47
	23.4[a]	5.1[a]	296	
JUC-141	21.6[a]	4.2[a]	273	S48
	27.6[a]	8.7[a]	298	
NOTT-202a	26.7[a]	2.9[b]	273	S31
	4.3[b]	1.4[b]	293	
MAF-66	403[b]	7.5[b]	273	S49
	225[b]	5.8[b]	298	
Cu-SSZ13(zeolite)	67.4[a]	NA	296	S34
H-SSZ13(zeolite)	71.3[a]	NA	296	S34
Zeolite MF1	11.2[a]	2.5[a,d]	296	S34
NaX zeolite	145.9[a]	60[a,d]	296	S34
JBW zeolite	524.4[a]	685.5[a,d]	296	S34

a: IAST selectivity; b: selectivity from Henry's Law; c: from slopes of adsorption isotherms at low pressure; d: selectivity at 2 bar.

References:

S1 H. Alawisi, B. Li, Y. He, H. D. Arman, A. M. Asiri, H. Wang and B. Chen, *Cryst. Growth Des*., 2014, **14**, 2522–2526.

S2 S. Chand, A. Pal and M. C. Das, *Chem. - A Eur. J.*, 2018, 5982–5986.

S3 A. Pal, S. Chand and M. C. Das, *Inorg. Chem.*, 2017, **56**, 13991–13997.

S4 A. Pal, S. Chand, S. M. Elahi and M. C. Das, *Dalt. Trans.*, 2017, **46**, 15280–15286.

S5 Z. Zhang, S. Xiang, K. Hong, M. C. Das, H. D. Arman, M. Garcia, J. U. Mondal, K. M. Thomas and B. Chen, *Inorg. Chem.*, 2012, **51**, 4947–4953.

S6 R.-J. Li, M. Li, X.-P. Zhou, D. Li and M. O'Keeffe, *Chem. Commun.*, 2014, **50**, 4047–4049.

S7 P. Deria, J. E. Mondloch, E. Tylianakis, P. Ghosh, W. Bury, R. Q. Snurr, J. T. Hupp and O. K. Farha, *J. Am. Chem. Soc.*, 2013, **135**, 16801–16804.

S8 B. Xiao, T. L. Easun, A. Dhakshinamoorthy, I. Cebula, P. H. Beton, J. J. Titman, H. Garcia, K. M. Thomas and M. Schröder, *J. Mater. Chem. A*, 2014, **2**, 19889–19896.

S9 D. Zhao, X.-H. Liu, J.-H. Guo, H.-J. Xu, Y. Zhao, Y. Lu and W.-Y. Sun, , *Inorg. Chem*., 2018, **57**, 2695–2704.

S10 Y. Ling, M. Deng, Z. Chen, B. Xia, X. Liu, Y. Yang, Y. Zhou and L. Weng, *Chem. Commun*., 2013, **49**, 78–80.

S11 W. M. Bloch, R. Babarao, M. R. Hill, C. J. Doonan and C. J. Sumby, *J. Am. Chem. Soc.*, 2013, **135**, 10441–10448.

S12 P. Nugent, Y. Belmabkhout, S. D. Burd, A. J. Cairns, R. Luebke, K. Forrest, T. Pham, S. Ma, B. Space, L. Wojtas, M. Eddaoudi and M. J. Zaworotko, *Nature*, 2013, **495**, 80–84.

S13 H. H. Wang, L. Hou, Y. Z. Li, C. Y. Jiang, Y. Y. Wang and Z. Zhu, *ACS Appl. Mater. Interfaces*, 2017, **9**, 17969–17976.

S14 C.-Y. Gao, H.-R. Tian, J. Ai, L.-J. Li, S. Dang, Y.-Q. Lan and Z.-M. Sun, *Chem. Commun.*, 2016, **52**, 11147–11150.

S15 H. J. Park, D. W. Lim, W. S. Yang, T. R. Oh and M. P. Suh, *Chem. - A Eur. J.*, 2011, **17**, 7251–7260.

S16 Z. Lu, L. Du, B. Zheng, J. Bai, M. Zhang and R. Yun, *CrystEngComm*, 2013, **15**, 9348.

S17 A. Demessence, D. M. D'Alessandro, M. L. Foo, J. R. Long, D. M. D'Alessandro, M. L. Foo and J. R. Long, *J. Am. Chem. Soc.*, 2009, **131**, 8784–8786.

S18 B. Li, Z. Zhang, Y. Li, K. Yao, Y. Zhu, Z. Deng, F. Yang, X. Zhou, G. Li, H. Wu, N. Nijem, Y. J. Chabal, Z. Lai, Y. Han, Z. Shi, S. Feng and J. Li, *Angew. Chemie - Int. Ed.*, 2012, **51**, 1412–1415.

S19 D. Lässig, J. Lincke, J. Moellmer, C. Reichenbach, A. Moeller, R. Gläser, G. Kalies, K. A. Cychosz, M. Thommes, R. Staudt and H. Krautscheid, *Angew. Chemie - Int. Ed.*, 2011, **50**,

10344–10348.

S20 P. Cui, Y. G. Ma, H. H. Li, B. Zhao, J. R. Li, P. Cheng, P. B. Balbuena and H. C. Zhou, *J. Am. Chem. Soc.*, 2012, **134**, 18892–18895.

S21 S. R. Caskey, A. G. Wong-Foy and A. J. Matzger, Department, *J. Am. Chem. Soc.*, 2008, **130**, 10870–10871.

S22 J. S. Choi, W. J. Son, J. Kim and W. S. Ahn, *Microporous Mesoporous Mater.*, 2008, **116**, 727–731.

S23 B. Mu, P. M. Schoenecker and K. S. Walton, *J. Phys. Chem. C*, 2010, **114**, 6464–6471.

S24 J. Jiao, L. Dou, H. Liu, F. Chen, D. Bai, Y. Feng, S. Xiong, D.-L. Chen and Y. He, *Dalton Trans*., 2016, **45**, 13373–13382.

S25 J. R. Li, J. Yu, W. Lu, L. B. Sun, J. Sculley, P. B. Balbuena and H. C. Zhou, *Nat. Commun.*, 2013, **4**, 1538.

S26 H. He, F. Sun, B. Aguila, J. A. Perman, S. Ma and G. Zhu, *J. Mater. Chem. A*, 2016, **4**, 15240–15246.

S27 L. Bastin, P. S. Ba, E. J. Hurtado, A. C. Silva, A. E. Rodrigues and B. Chen, *J. Phys. Chem. C*, 2008, **112**, 1575–1581.

S28 Z. Liang, M. Marshall and A. L. Chaffee, *Energy and Fuels*, 2009, 2785–2789.

S29 C. Tan, S. Yang, N. R. Champness, X. Lin, A. J. Blake, W. Lewis and M. Schröder, *Chem. Commun.*, 2011, **47**, 4487.

S30 P. L. Llewellyn, S. Bourrelly, C. Serre, A. Vimont, M. Daturi, L. Hamon, G. De Weireld, J. Chang, D. Hong, Y. K. Hwang and S. H. Jhung, *Langmuir*, 2008, 7245–7250.

S31 S. Yang, X. Lin, W. Lewis, M. Suyetin, E. Bichoutskaia, J. E. Parker, C. C. Tang, D. R. Allan, P. J. Rizkallah, P. Hubberstey, N. R. Champness, K. Mark Thomas, A. J. Blake and M. Schröder, *Nat. Mater.*, 2012, **11**, 710–716.

S32 O. Yazaydin, A. I. Benin, S. a Faheem, P. Jakubczak, J. J. Low, R. R. Willis and R. Q. Snurr, *Chem. Mater.*, 2009, **21**, 1425–1430.

S33 B. Zheng, J. Bai, J. Duan, L. Wojtas and M. J. Zaworotko, *J. Am. Chem. Soc.*, 2011, **133**, 748–751.

S34 S. Xiang, Y. He, Z. Zhang, H. Wu, W. Zhou, R. Krishna and B. Chen, *Nat. Commun.*, 2012, **3**, 954–959.

S35 S. Xiong, Y. Gong, H. Wang, H. Wang, Q. Liu, M. Gu, X. Wang, B. Chen and Z. Wang, *Chem. Commun.*, 2014, **50**, 12101–12104.

S36 H. Alawisi, B. Li, Y. He, H. D. Arman, A. M. Asiri, H. Wang and B. Chen, *Cryst. Growth Des.*, 2014, **14**, 2522–2526.

S37 O. Alduhaish, H. Wang, B. Li, H. D. Arman, V. Nesterov, K. Alfooty and B. Chen, *Chempluschem*, 2016, **81**, 764–769.

S38 A. Phan, C. J. Doonan, F. J. Uribe-Romo, C. B. Knobler, M. O'Keeffe and O. M. Yaghi, *Acc Chem Res*, 2010, **43**, 58–67.

S39 A. Pal, J. Bin Lin, S. Chand and M. C. Das, *ChemistrySelect*, 2018, **3**, 917–921.

S40 P. Nugent, V. Rhodus, T. Pham, B. Tudor, K. Forrest, L. Wojtas, B. Space and M. Zaworotko, *Chem. Commun.*, 2013, **49**, 1606.

S41 T. M. McDonald, D. M. D'Alessandro, R. Krishna and J. R. Long, *Chem. Sci.*, 2011, **2**, 2022.

S42 T. M. McDonald, W. R. Lee, J. A. Mason, B. M. Wiers, C. S. Hong and J. R. Long, *J. Am. Chem. Soc.*, 2012, **134**, 7056–7065.

S43 J. Li, G. P. Yang, S. L. Wei, R. C. Gao, N. N. Bai and Y. Y. Wang, *Cryst. Growth Des.*, 2015, **15**, 5382–5387.

S44 Z. J. Lin, Y. B. Huang, T. F. Liu, X. Y. Li and R. Cao, *Inorg. Chem.*, 2013, **52**, 3127–3132.

S45 Y.-L. Huang, D.-C. Zhong, L. Jiang, Y.-N. Gong and T.-B. Lu, *Inorg. Chem.*, 2017, **56**, 705–708.

S46 C. Song, J. Hu, Y. Ling, Y. Feng, R. Krishna, D. Chen and Y. He, *J. Mater. Chem. A*, 2015, **3**, 19417–19426.

S47 O. Alduhaish, H. Wang, B. Li, T. L. Hu, H. D. Arman, K. Alfooty and B. Chen, *Chempluschem*, 2016, **81**, 770–774.

S48 N. Zhao, F. Sun, P. Li, X. Mu and G. Zhu, *Inorg. Chem.*, 2017, **56**, 6938–6942.

S49 R. B. Lin, D. Chen, Y. Y. Lin, J. P. Zhang and X. M. Chen, *Inorg. Chem.*, 2012, **51**, 9950–9955.